WILEY | Hindawi

Research Article

Investigation of Cortical Signal Propagation and the Resulting Spatiotemporal Patterns in Memristor-Based Neuronal Network

Ke Ding [iD],[1,2] **Zahra Rostami,**[3] **Sajad Jafari,**[3] **and Boshra Hatef** [iD][4]

[1]*School of Information Technology, Jiangxi University of Finance and Economics, Nanchang 330013, China*
[2]*Jiangxi E-Commerce High Level Engineering Technology Research Centre, Jiangxi University of Finance and Economics, Nanchang 330013, China*
[3]*Biomedical Engineering Department, Amirkabir University of Technology, Tehran 15875-4413, Iran*
[4]*Neuroscience Research Center, Baqiyatallah University of Medical Sciences, Tehran, Iran*

Correspondence should be addressed to Boshra Hatef; boshrahatef@gmail.com

Complexity is the undeniable part of the natural systems providing them with unique and wonderful capabilities. Memristor is known to be a fundamental block to generate complex behaviors. It also is reported to be able to emulate synaptic long-term plasticity as well as short-term plasticity. Synaptic plasticity is one of the important foundations of learning and memory as the high-order functional properties of the brain. In this study, it is shown that memristive neuronal network can represent plasticity phenomena observed in biological cortical synapses. A network of neuronal units as a two-dimensional excitable tissue is designed with 3-neuron Hopfield neuronal model for the local dynamics of each unit. The results show that the lattice supports spatiotemporal pattern formation without supervision. It is found that memristor-type coupling is more noticeable against resistor-type coupling, while determining the excitable tissue switch over different complex behaviors. The stability of the resulting spatiotemporal patterns against noise is studied as well. Finally, the bifurcation analysis is carried out for variation of memristor effect. Our study reveals that the spatiotemporal electrical activity of the tissue concurs with the bifurcation analysis. It is shown that the memristor coupling intensities, by which the system undergoes periodic behavior, prevent the tissue from holding wave propagation. Besides, the chaotic behavior in bifurcation diagram corresponds to turbulent spatiotemporal behavior of the tissue. Moreover, we found that the excitable media are very sensitive to noise impact when the neurons are set close to their bifurcation point, so that the respective spatiotemporal pattern is not stable.

1. Introduction

The brain is composed of an extremely large number of neurons [1], as the basic and also complex adaptive blocks of the brain system [2, 3]. Neuronal information transference is possible via propagation of the electrical and chemical signals in neuronal network [4, 5]. Indeed, fluctuation of the membrane potential of the neurons has a specific pattern in both time domain and space domain within the information processing [6]. These fluctuations actually bring a functional coherence and interplay between different parts, so that the related controlling behaviors are possible [7]. It is confirmed that emergence of a particular spatiotemporal pattern is in direct relationship with the intrinsic properties of the system [6, 8, 9]. Metabolically, generation and transference of the information and the related signals are costly [4, 10]. However, the way that the brain is wired has made it a nature-made computer with high level of efficiency in computation and cognition [4]. Although the human brain is not very quick at handling complex calculations, it beats a traditional computer system when it comes to energy efficiency [11]. Therefore, many efforts have been made to build up a hardware structure and a software design or even employ a mathematical model to study the brain system [12, 13], regarding some functional

properties or physical effects [14]. There can be considered some factors responsible for energy efficiency of neuronal network including mechanisms of action potential propagation, synaptic neurotransmitters, and other factors that are studied in more detail in [4]. In this regard, it is interesting to investigate the emerged spatiotemporal patterns accompanied by the complex dynamics [8]. The recent studies on neural network and emulator circuit implementations [13–15] have led to the fourth circuit element called memristor [16] in addition to resistor, capacitor, and inductor [15, 17, 18]. Memristor (contraction of memory and resistor) is a two-terminal circuit element with nonlinear characteristics and high performance [19]. It has attracted much attention in biological models, adaptive filters, or integrated circuits [20] due to multistability phenomenon in coexisting attractors with chaotic demonstrations [21]. For the application of biological models, it can mimic how neurons in a network change their behavior when they are activated. Actually, its respond at each moment does not rely only on the signals it is receiving at that exact moment but is influenced by its own recent activity, too.

Many studies prove that biological behaviors are the outcome of collective activities of the neurons in neural network [22]. Indeed, the brain activities are not determined by each individual neuron, separately, but the intrinsic coherence coming from collective activities and patterns of maintenance or destruction of the local synchronization between the agents [23, 24]. As a result, it is not only about the components and their fluctuation pattern, individually, but also about the connections among them. In other words, neuronal information is carried by evolutionary spatiotemporal patterns indicating a powerful, efficient, and purposeful functional connectivity. Besides, the connection strength determines the specific spatial patterns in the network, as well [24]. Actually, what seems to have the most significant and delicate influence over the ultimate performance of the system is the interactions between the components, both quantitatively and qualitatively. Thus, we need to know the spatiotemporal distribution of the brain cells membrane potential and the pattern of propagated waves in the two-dimensional space focusing on the connections [8]. However, obviously, association of a large number of unites within nonlinear connections and interactions makes it so hard to grasp some of the concepts and deal with the related topics. Therefore, some simplifications with acceptable range of reductions are needed [25]. Regardless of these reductions in what is actually happening in the real neuronal network, this procedure can help us understand the related complicated occurrence, to some extent. In this study, the main idea is to notice the neurons at the level of population and consider a group of correlated neurons within more realistic interconnections and communication tools.

The point at which neurons are able to communicate with each other is called synapse [3], which bridges the neurons in the neuronal network [26]. In fact, transmission of the electrical signal in neuronal system can take place through synapses. It is also found that learning and memory are the two significant brain abilities attributed to synapses and their functional properties [3]. From a perspective, learning and memory are interrelated with each other. Memory is the internal mental recorded information, while learning is the ability of modifying the information stored in the memory based on the new inputs. More precisely, it also can be said that learning is the first step of memory since the sensory system sends information to the brain. Synaptic plasticity is postulated to be one of the important foundations of learning and memory [27]. Furthermore, plasticity is reported to be responsible for certain abilities like rapid response to threat stimuli and localization of the sound source [28]. The invention of memristor has made it possible to realize some complex activities which were impeded by lack of an appropriate device to model synaptic plasticity. The focus of this study is to demonstrate the capability of memristive neuronal network to represent some complex behaviors and large-scale plasticity which is also well described via experimental observations in the prefrontal cortex [29], visual cortex [30], and neocortex [31].

Real cortical tissue has a laminar structure [32]. Indeed, neurons of cerebral cortex are arranged in characteristic layers [3]. Primarily, presence or absence of neuronal cell bodies specifies the layers of cerebral cortex. This laminar structure of the cortex plays a significant role in organizing the inputs and outputs of the brain [3]. In fact, different inputs need to be processed in different ways while the outputs arise from different cortical regions. Accordingly, the laminar structure of cerebral cortex helps providing required circumstances. Considering distribution of the cortical electrical activities, related spatiotemporal patterns arise from the interface between the levels of activities of neurons in the surfaces. With given explanations, in this study, we simplify the case to a two-dimensional network of neuronal models, expressing an excitable cortical tissue to investigate the resulting pattern of the wave propagation in the surface.

In order to study the factors affecting wave propagation, it is interesting to figure out what a memristor-type synaptic connection exactly does, not only for one limited agent but also for large number of neuronal units and how much it affects the spatial distribution of the cell membrane potential and leads to wave propagation via the complex demonstrations. Actually, the answer of these questions may also reflect the influence of memory and learning process in a neuronal network through the emerged patterns. In other words, we examine different plasticity levels for the synaptic connections by means of different memristor contributions. On the other hand, by noticing differential equation models, which are used in this study, the initial states of the variables of a system refer to the result of their past dynamics. Therefore, we choose a different initial condition for a local area of the network indicating the different input sensory signals that have been applied to that specific area in the past. After that, we investigate the effect of memristor-type synapse against resistor-type synapse on the pattern formation in the network. Plus, we also expand our computations to noise considerations in some separated snapshots, because noise plays an important role in dynamical response of oscillatory systems.

The results show that different spatiotemporal patterns take place in the excitable tissue without supervision. As is

clear through the snapshots, the overall pattern is mostly determined by memristor-type coupling. In accordance with some reports on the role of synaptic plasticity in some important high-order cortical activities, our results confirm that synaptic plasticity makes the tissue capable of representing different complex demonstrations. In fact, the increase and decrease of the memristor effect greatly changes the ultimate appearance of the tissue, which, in turn, actually resulted from the pattern of electrical activity of each neuron interacting with the neighbor neurons in the whole tissue. Moreover, the resulting patterns are found to be robust against noise for all the cases except for $k = 0.9$, in which some concentric circular patterns are formed in the two-dimensional space. For further study, we sought to realize whether it is possible to find a meaningful relationship between the qualitative properties of the coupled neurons and the spatiotemporal demonstrations from a two-dimensional lattice. Therefore, the bifurcation analysis is carried out for different intensities of memristor-type coupling. It is revealed that the spatiotemporal electrical activity of the tissue concurs with the bifurcation analysis. We show the memristor coupling intensities by which the system undergoes periodic behavior and prevents the tissue from holding wave propagation. In addition, the chaotic-like behavior in bifurcation diagram corresponds to turbulent spatiotemporal behavior of the tissue. Moreover, it is found that the excitable media is very sensitive to noise impact when the neurons are set close to their bifurcation point, so that the respective spatiotemporal pattern is not stable.

The rest of the paper is organized as follows.

In the next section, the mathematical model is introduced with description of its variables and parameters. After that, in the third section, our numerical method is explained and the results are displayed. The computational analysis for variation of k and D can be found in Section 3.1. Sections 3.2 and 3.3 include the noise and the bifurcation analysis, respectively. Finally, the fourth section concludes our study.

2. Model and Description

There are a number of mathematical neural models capable of representing complex dynamic behaviors. These models introduced for a large number of neurons have properties that benefit investigations on biological neuronal network. Usually, in these models, it is assumed that the presynaptic firing rate determines the synaptic input current [33]. Hopfield neural model is defined as a graded response model [34]. This model has been successful in representing different dynamical behaviors including chaotic behaviors [35, 36] having to do with nonlinear demonstrations of the brain performance.

Neurons have a selective response to a compact range of parameters. In our study, the idea is to provide a compact range of connections and interactions in a neuronal network. For this purpose, we designed a square array of neuronal units with nearest neighbor connections. Each unit has a topology with hyperbolic-type memristor-based connection. A hyperbolic-type Hopfield neural network is considered for each agent. In this 3-neuron Hopfield neural network, one of the connection weights is defined as a memristive-type

weight. The Hopfield equation for the i-th neuron is described as follows:

$$C_i \frac{dx_i}{dt} = -\frac{x_i}{R_i} + \sum_{j=1}^{N} w_{ij} \tanh\left(x_i\right) + I_i, \tag{1}$$

where variable x denotes the voltage across the capacitor C, R stands for membrane resistance between the inside and outside of the neuron, I is an input bias current, $\tanh(x_j)$ is the neuron activation function for voltage input from the j-th neuron, and w_{ij} is synaptic weight that illustrates the strength of connections between i-th and j-th neurons. In our work, the proposed Hopfield network is achieved by replacing resistive connection with hyperbolic-type memristor, which is discussed in detail in [35]. The set of parameters are $N = 3$, $C_i = 1, R_i = 1$ $(i = (1:3))$. The weight matrix is considered as

$$W = \begin{bmatrix} w_{11} & w_{12} & w_{13} \\ w_{21} & w_{22} & w_{23} \\ w_{31} & w_{32} & w_{33} \end{bmatrix} = \begin{bmatrix} -1.4 & 1.2 & -7 \\ 1.1 & 0 & 2.8 \\ kw & -2 & 4 \end{bmatrix}, \tag{2}$$

where w is the synaptic weight connecting the first and the third neurons with the proportion of k. The parameter k is a constant indicating the strength of hyperbolic-type memristor-type coupling.

The differential equations describing the desired memristor-type neuronal unit can be expressed as follows:

$$\dot{x}_1 = -x_1 - 1.4 \tanh\left(x_1\right) + 1.2 \tanh\left(x_2\right) - 7 \tanh\left(x_3\right)$$

$$\dot{x}_2 = -x_2 + 1.1 \tanh\left(x_1\right) + 2.8 \tanh\left(x_3\right)$$

$$\dot{x}_3 = -x_3 + kw \tanh\left(x_1\right) - 2 \tanh\left(x_2\right) + 4 \tanh\left(x_3\right) \tag{3}$$

$$\dot{x}_4 = -x_4 + \tanh\left(x_1\right)$$

$$w = a - b \tanh\left(x_4\right).$$

After that, we develop the case to a large array network of neuronal units within coupling intensities. Therefore, the equations for the square array network are represented as follows:

$$\dot{x}_{1_{mn}} = -x_{1_{mn}} - 1.4 \tanh\left(x_{1_{mn}}\right) + 1.2 \tanh\left(x_{2_{mn}}\right) - 7$$
$$\cdot \tanh\left(x_{3_{mn}}\right),$$

$$\dot{x}_{2_{mn}} = -x_{2_{mn}} + 1.1 \tanh\left(x_{1_{mn}}\right) + 2.8 \tanh\left(x_{3_{mn}}\right),$$

$$\dot{x}_{3_{mn}} = -x_{3_{mn}} + kw_{mn} \tanh\left(x_{1_{mn}}\right) - 2 \tanh\left(x_{2mn}\right) + 4$$
$$\cdot \tanh\left(x_{3_{mn}}\right) + D \tag{4}$$
$$\cdot \tanh\left(x_{3_{m-1n}} + x_{3_{m+1n}} + x_{3_{mn-1}} + x_{3_{mn+1}} - 4x_{3_{mn}}\right),$$

$$\dot{x}_{4_{mn}} = -x_{4_{mn}} + \tanh\left(x_{1_{mn}}\right),$$

$$w_{mn} = a - b \tanh\left(x_{4_{mn}}\right),$$

where the subscript mn denotes the position of each neuronal unit in the two-dimensional square array network. D is the
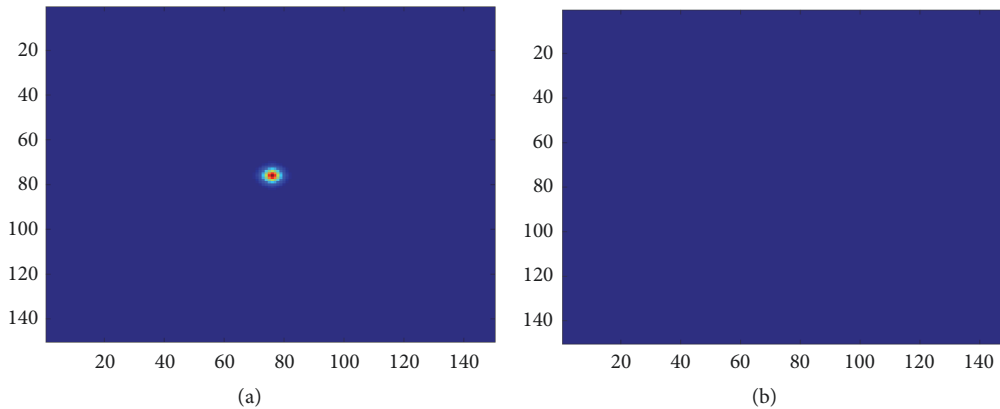
FIGURE 1: The snapshots of spatial distribution of membrane potential with color scale for neurons in the square array network for $k = 0$ and $D = 1$ at (a) $t = 2$ time units and (b) $t = 6$ time units.

resistor-type coupling intensity. $a = 1$ and $b = 0.01$ are constant. The reader will pay attention that the parameter D denotes the resistor-type coupling strength in this study while parameter k shows the memristor-type coupling strength.

3. Numerical Results and Discussions

In our study, we design a square array network consisting of 150×150 neuronal units. Our numerical results are calculated by Runge-Kutta 4th-order method with the time step $h = 0.01$ under no flux boundary. The initial states of the network except the small central area, which is observable in the following images, are set as $(x_1, x_2, x_3, x_4) = (0, 0.1, 0, 0)$. In addition, the initial condition of the central local area is $(x_1, x_2, x_3, x_4) = (0, -0.1, 0, 0)$.

3.1. Computational Analysis for Variation of k and D. Considering (2), there are two types of coupling between neurons in the whole network, namely, the memristor-type coupling and the resistor-type coupling. We pick different levels of memristor-type coupling by adjusting parameter k, and then we consider two levels of resistor-type coupling intensity by adjusting parameter D, in each case of k adjustments.

It seems that neurons need to have an appropriate level of memristor effect to be capable of responding to the received stimulus in a desired pattern leading to wave propagation. Otherwise, the generated circular wave (in the central area of the network) will not be developed. Even though a propagated wave can travel a further distance by strengthening the resistive coupling intensity between the agents (which is adjustable by parameter D), still the lack of wave propagation remains and the ultimate general pattern does not change. Moreover, the excitable media are able to switch over different spatial behaviors by varying the memristive coupling strength. Hence, from this point of view, memristor-type coupling is more noticeable against resistor-type coupling. To put it more clearly, the distribution of membrane potential in the two-dimensional excitable media is shown in colored levels. In some cases, the central local area is maintained for a few seconds or continues to grow

under a particular pattern, while in others the continuity of the central part is very short.

Firstly, Figure 1 shows the result in two snapshots when there is no effect of memristor in the network ($k = 0$). Moreover, the neuronal units are connected to each other with the coupling intensity of $D = 1$. As it is observable, there is no propagation in this case and the generated signals find no path to travel the tissue. In fact, the generated wave front dies right at the beginning of its existence. Besides, there is no sign of propagation even when we choose a higher resistor-type coupling intensity by $D = 5$ under no memory effect by $k = 0$ (Figure 2). Here the only difference that can be seen between the results in Figures 1 and 2 is in the increased radius of the initiated wave front in Figure 2 in comparison with Figure 1. In this case, the central concentrated energy does not flow to the rest of the neurons and vanishes right at the beginning of its existence.

For the next step, we provide the tissue a nonzero memory effect with $k = 0.5$ under resistor coupling strength of $D = 1$ and $D = 5$ displayed in Figures 3 and 4, respectively. In this case, the membrane potential of the central local area finds permission to flow beyond the central part but not too far. The propagated wave is shown in four snapshots for this case. As it is observable, in this case, the wave front disappears not right at the beginning but after a limited time before getting too wide (see Figure 3). Moreover, increasing the resistor-type coupling intensity from $D = 1$ to $D = 5$ only brings the time-limited propagated wave a greater radius and does not prevent it from disappearing (see Figure 4).

After that, on the way of increasing memory properties, leading to more synaptic plasticity, we set $k = 0.7$ (Figures 5 and 6). Interestingly, this slight increase from $k = 0.5$ to $k = 0.7$ in the level of memory effects brings out significantly different dynamics from the tissue. In fact, it makes the tissue represent a very distinctive pattern for the distribution of membrane potential in its two-dimensional space. The spatial fluctuations become so turbulent and great number of very small rotating seeds can be seen. These countless rotating seeds result in such turbulent appearance as is clear through the depicted snapshots in Figures 5 and 6. We investigate
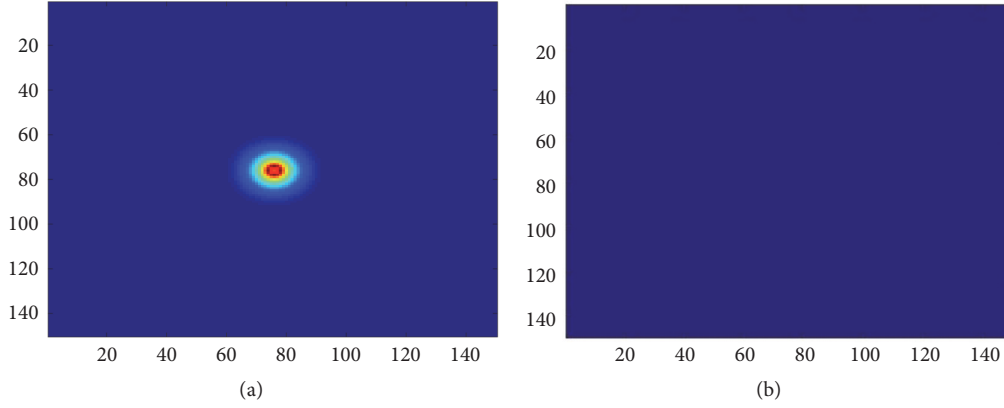
FIGURE 2: The snapshots of spatial distribution of membrane potential with color scale for neurons in the square array network for $k = 0$ and $D = 5$ at (a) $t = 2$ time units and (b) $t = 6$ time units.
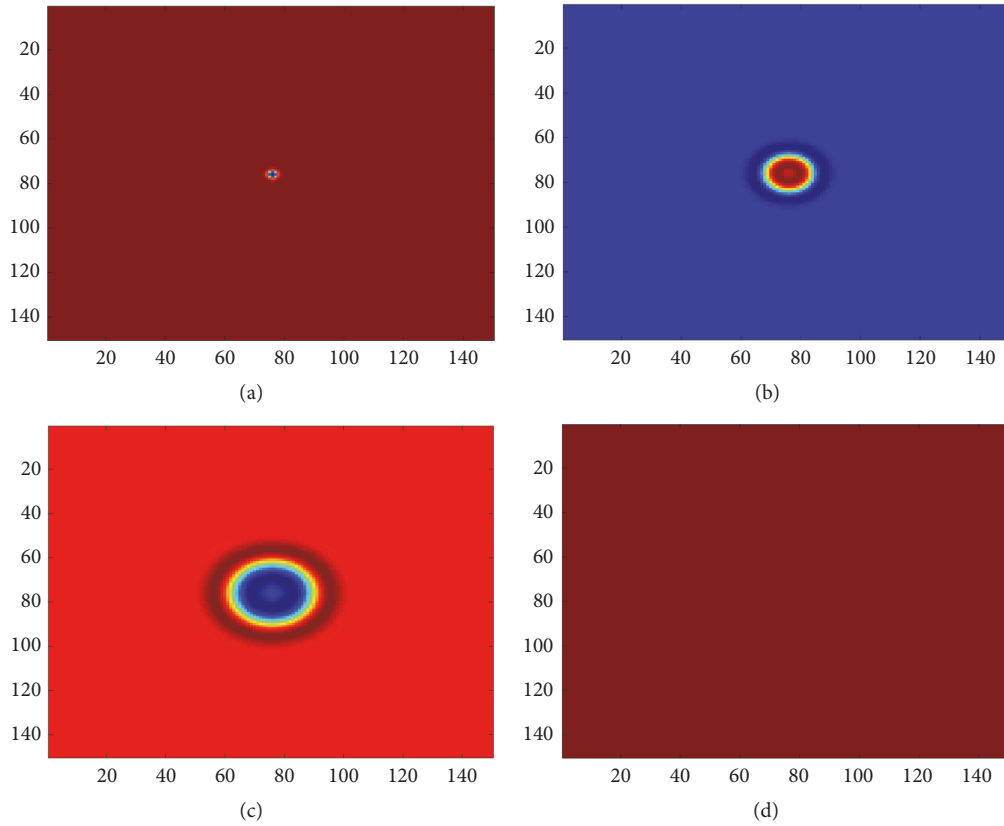

FIGURE 3: The snapshots of spatial distribution of membrane potential with color scale for neurons in the square array network for $k = 0.5$ and $D = 1$ at (a) $t = 2$ time units, (b) $t = 20$ time units, (c) $t = 100$ time units, and (d) $t = 200$ time units.

this level of memory effects with two resistance coupling intensities by $D = 1$ and $D = 5$ and the resulting snapshots are displayed in Figures 5 and 6, respectively. As before, greater amounts of parameter D cause the radius of the turbulent propagating wave increase, so that a more extensive area is covered in the snapshots of the same moments.

Furthermore, we examine a slightly further increase in the level of memory effects by applying $k = 0.8$ in two modes of $D = 1$ and $D = 5$. The resulting spatiotemporal patterns are shown in Figures 7 and 8, respectively. As it is observable, in this case, the regular symmetrical deformations are surrounded by a growing circular wave front. As soon as the circular wave front touches the boundaries, it starts getting into some deformations, too. Eventually, the mixture of the resulting deformations covers the entire tissue and makes it represent a completely different appearance (Figure 7(d)).

Considering all the above, we set a higher level of memristor-type coupling by $K = 0.9$, in order to see whether
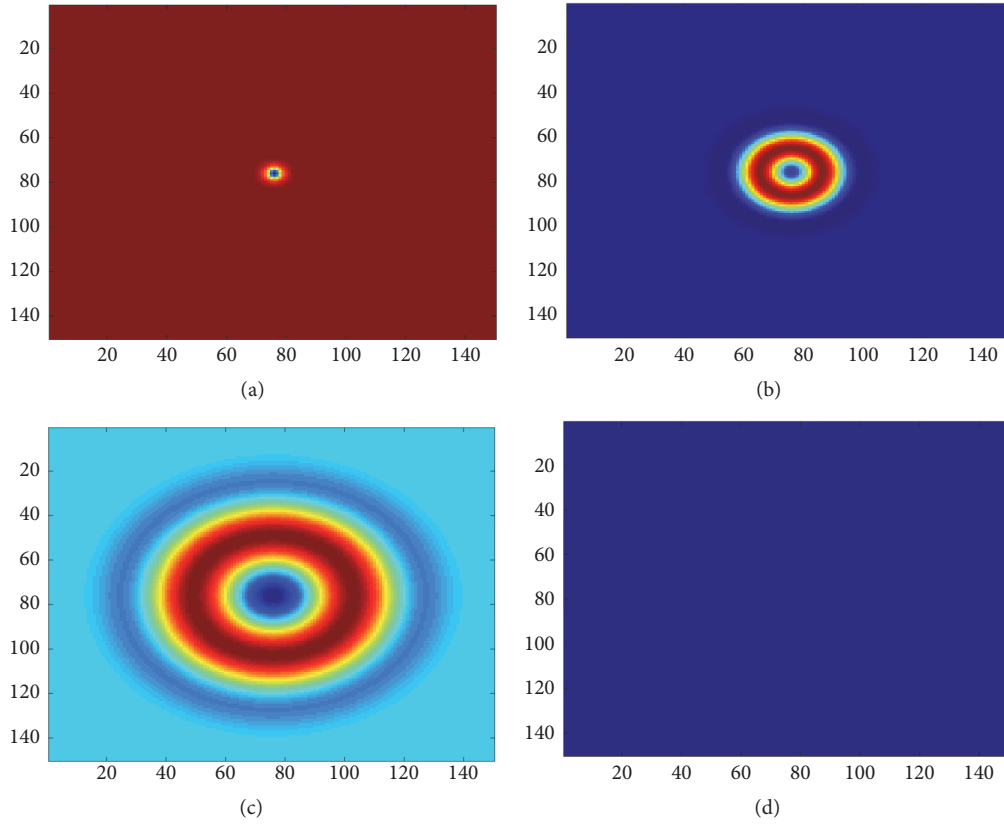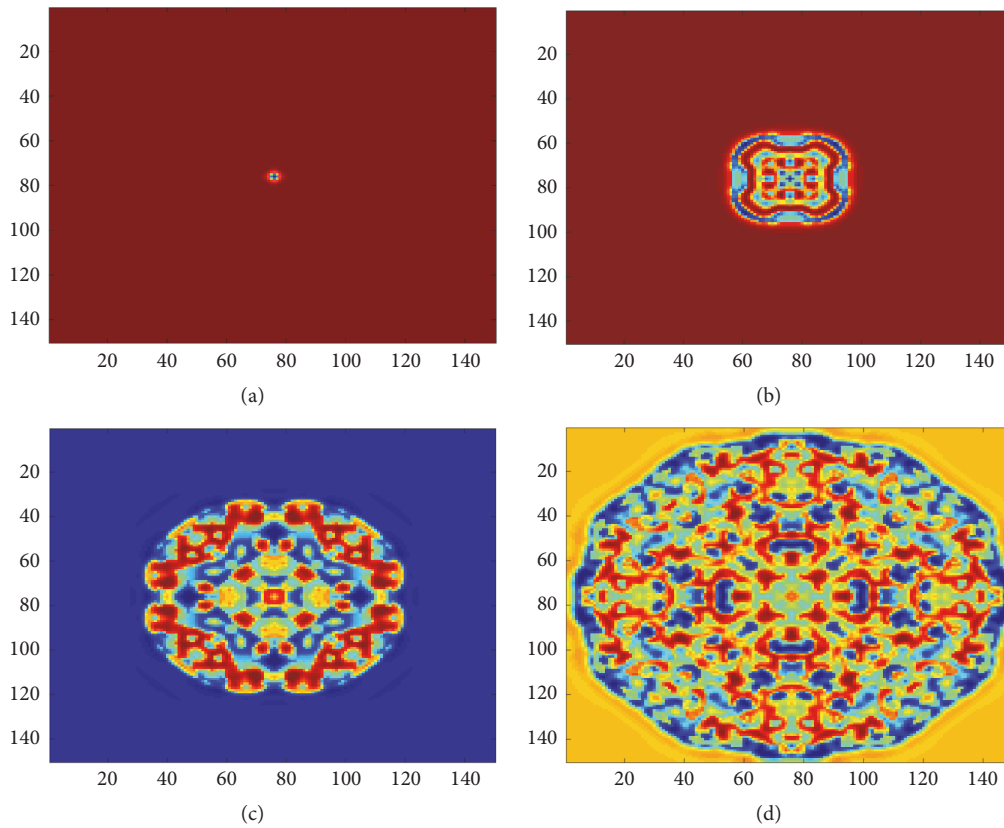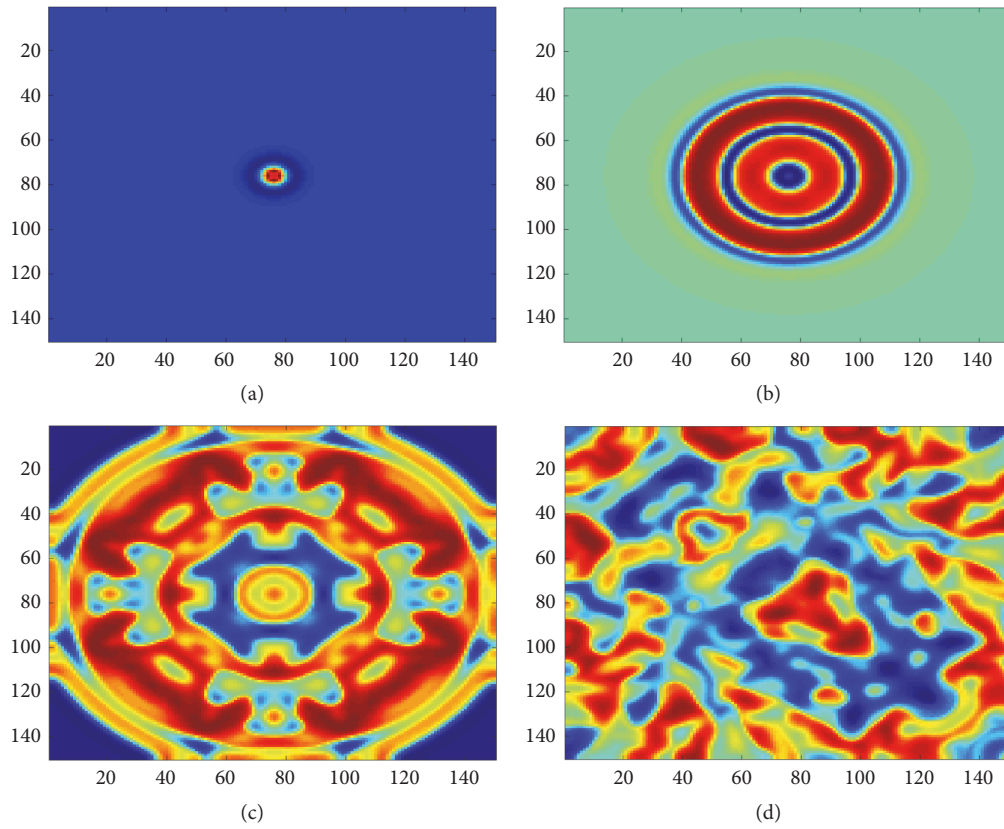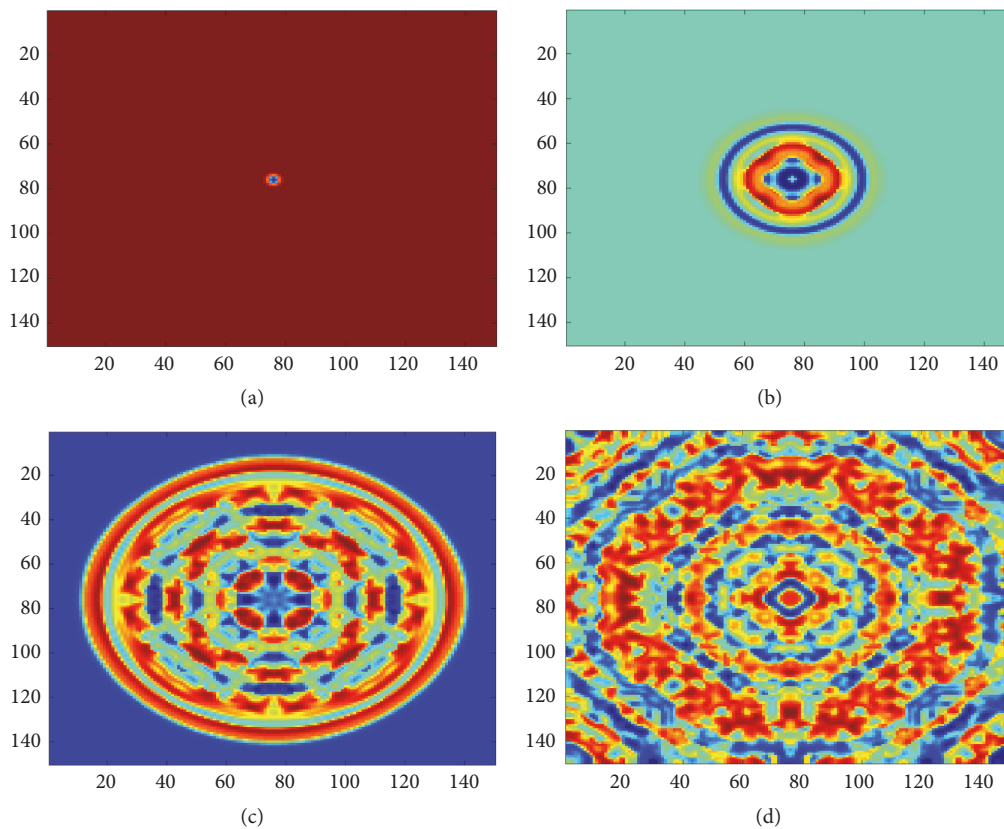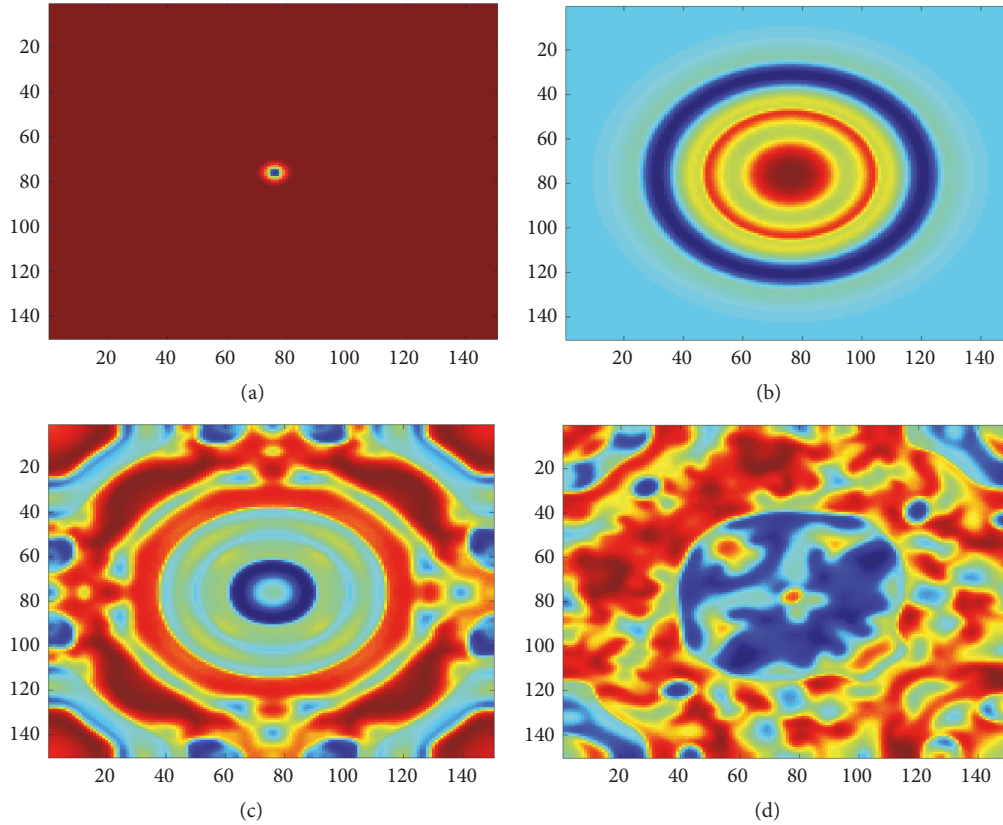
FIGURE 4: The snapshots of spatial distribution of membrane potential with color scale for neurons in the square array network for $k = 0.5$ and $D = 5$ at (a) $t = 2$ time units, (b) $t = 20$ time units, (c) $t = 100$ time units, and (d) $t = 200$ time units.

FIGURE 5: The snapshots of spatial distribution of membrane potential with color scale for neurons in the square array network for $k = 0.7$ and $D = 1$ at (a) $t = 2$ time units, (b) $t = 75$ time units, (c) $t = 170$ time units, and (d) $t = 300$ time units.

Figure 6: The snapshots of spatial distribution of membrane potential with color scale for neurons in the square array network for $k = 0.7$ and $D = 5$ at (a) $t = 2$ time units, (b) $t = 75$ time units, (c) $t = 135$ time units, and (d) $t = 300$ time units.

Figure 7: The snapshots of spatial distribution of membrane potential with color scale for neurons in the square array network for $k = 0.8$ and $D = 1$ at (a) $t = 2$ time units, (b) $t = 75$ time units, (c) $t = 170$ time units, and (d) $t = 300$ time units.

(a)

(b)

(c)

(d)

FIGURE 8: The snapshots of spatial distribution of membrane potential with color scale for neurons in the square array network for $k = 0.8$ and $D = 5$ at (a) $t = 2$ time units, (b) $t = 75$ time units, (c) $t = 135$ time units, and (d) $t = 300$ time units.

the resulting turbulent pattern continues to grow by more strengthening the memristor-type coupling in the network. The results are represented for $D = 1$ and $D = 5$ in Figures 9 and 10, respectively.

As is visible in the displayed results in Figures 9 and 10, the spatial pattern takes a completely different appearance when we pick the strength of memristor-type coupling beyond a certain threshold. Besides, there is no sign of any small rotating seeds either. In this case, with this set of parameters, the central local area does not vanish and there exist a set of concentric circles. Unlike the previous cases, these arising circular wave fronts keep their overall curvature during the whole time span. Moreover, these circular wave fronts take a larger radius and find more expansion when the resistor-type coupling is increased from $D = 1$ to $D = 5$ (Figure 10). As a result, this level of memristor effect causes a recognizable change in the resulting spatiotemporal behavior. Even though more synaptic plasticity is provided in this case, the turbulent spatial pattern changes into a circular discipline with no deformation.

For further investigation, we put the memory influence of the excitable tissue in a higher level by setting $k = 1$ with $D = 1$ and $D = 5$ in Figures 11 and 12, respectively. Interestingly, neither partial deformation nor circular pattern is observable in this case. Besides, the ultimate wave front stops to grow after reaching a certain length of the radius.

Moreover, by further increase of the memory level by $k = 1.5$, the propagated wave subsides and finally disappears. For this level of k, the snapshots in Figures 13 and 14 show the results for $D = 1$ and $D = 5$, respectively.

3.2. Noise Effect. In this part, we expand our computational analysis to investigate stability of the emerged patterns under the noise effect. For this purpose, the Gaussian white noise $\xi(t)$ is added to the initial conditions, which were defined in the first paragraph of Section 3. The statistical properties of Gaussian white noise are defined by [37]

$$\langle \xi(t) \xi(t') \rangle = 2G\delta(t - t'), \qquad (5)$$

where G is noise intensity and $\delta(*)$ is Dirac-δ function. Two levels of noise intensities are applied to the whole tissue by $G = 0.01$ and $G = 0.1$.

The results show that the spatial pattern totality is not influenced by the noise effect for $k = 0$, $k = 0.5$, $k = 0.7$, $k = 0.8$, $k = 1$, and $k = 1.5$, so that the ultimate spatial pattern does not change significantly for these cases. These results are depicted in Figures 15–18, 20 and 21. However, as illustrated in Figure 19, in the case $k = 0.9$, a remarkable change is made in the network fluctuations pattern due to the noise effects. It seems that this level of memristor-type coupling makes the tissue sensitive to noise and makes it represent a
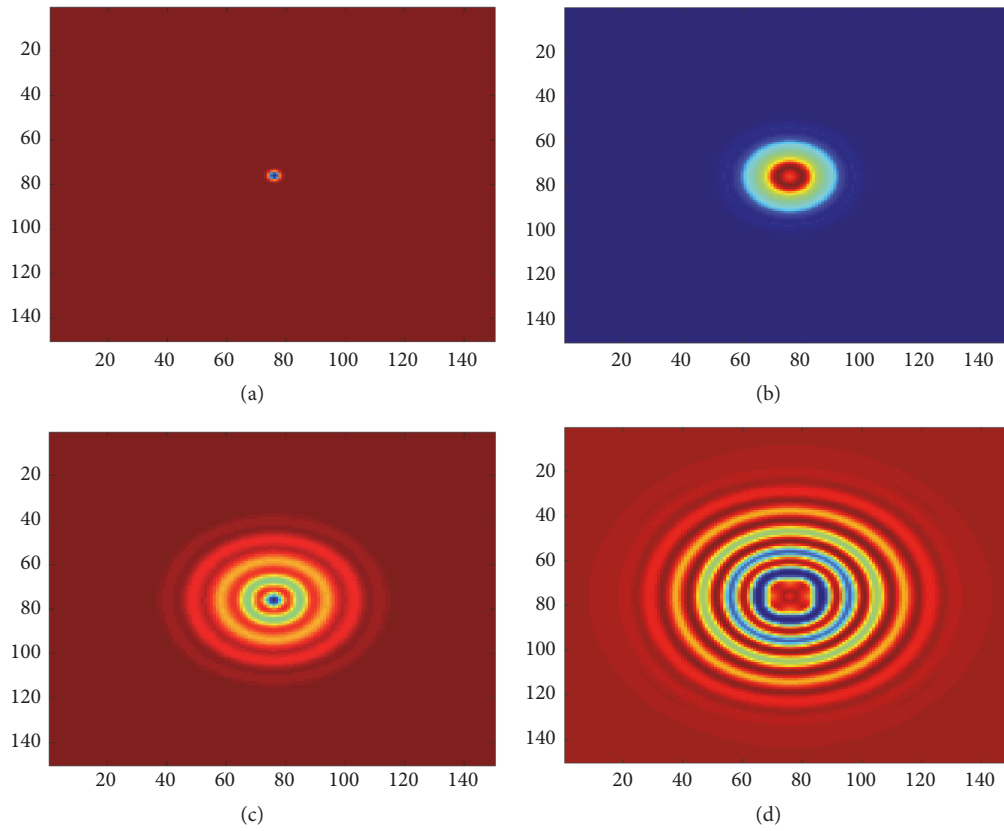
FIGURE 9: The snapshots of spatial distribution of membrane potential with color scale for neurons in the square array network for $k = 0.9$ and $D = 1$ at (a) $t = 2$ time units, (b) $t = 75$ time units, (c) $t = 170$ time units, and (d) $t = 300$ time units.
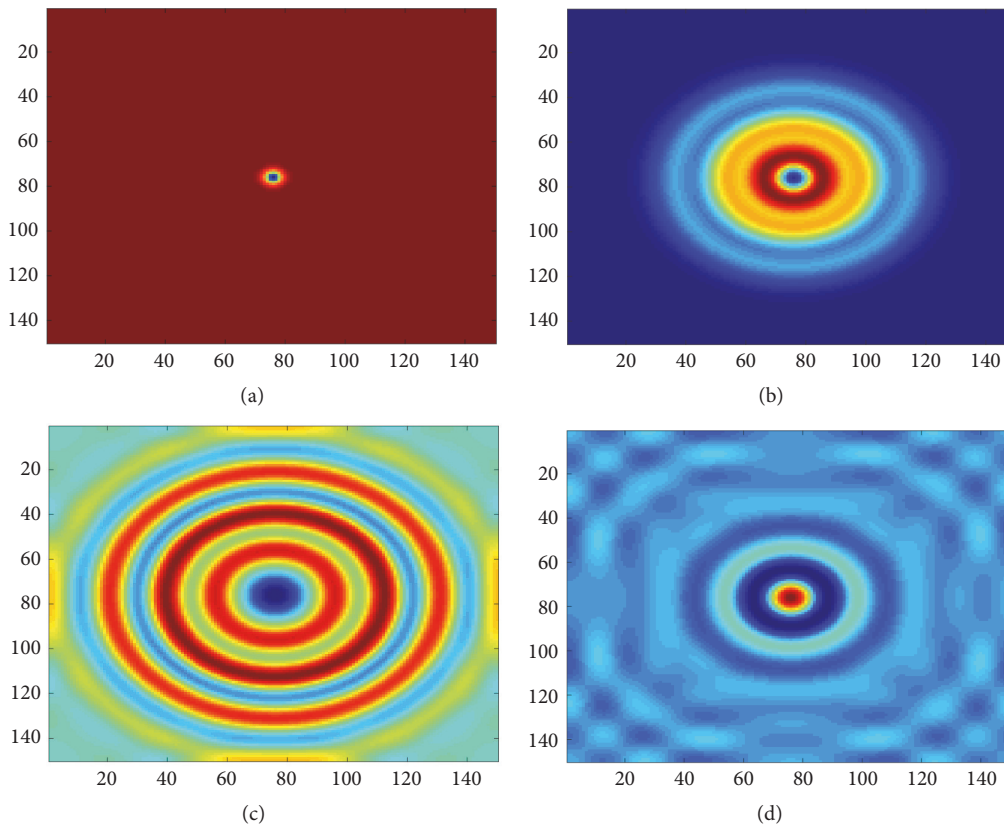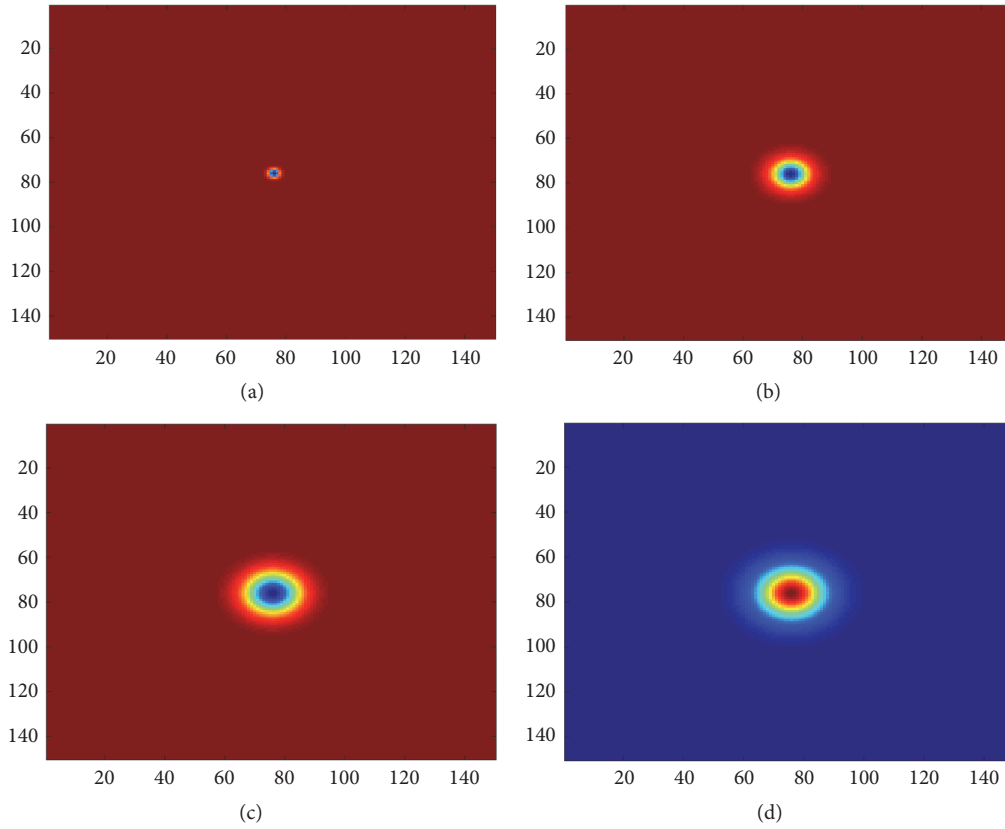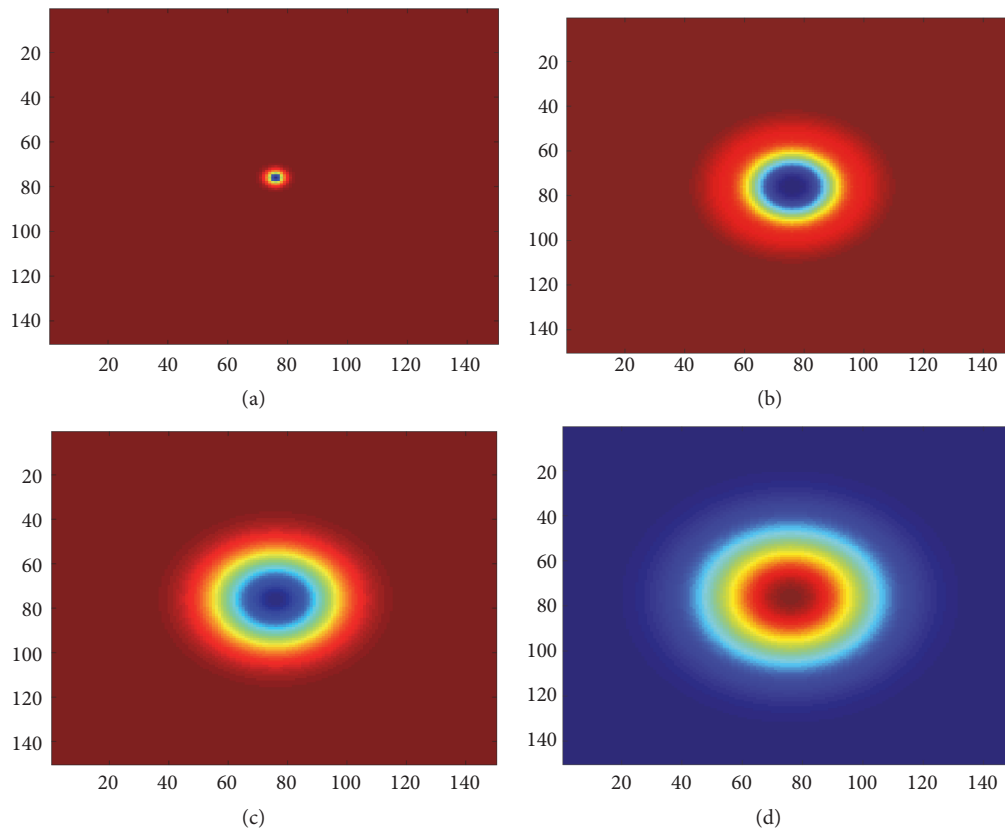

FIGURE 10: The snapshots of spatial distribution of membrane potential with color scale for neurons in the square array network for $k = 0.9$ and $D = 5$ at (a) $t = 2$ time units, (b) $t = 75$ time units, (c) $t = 135$ time units, and (d) $t = 300$ time units.
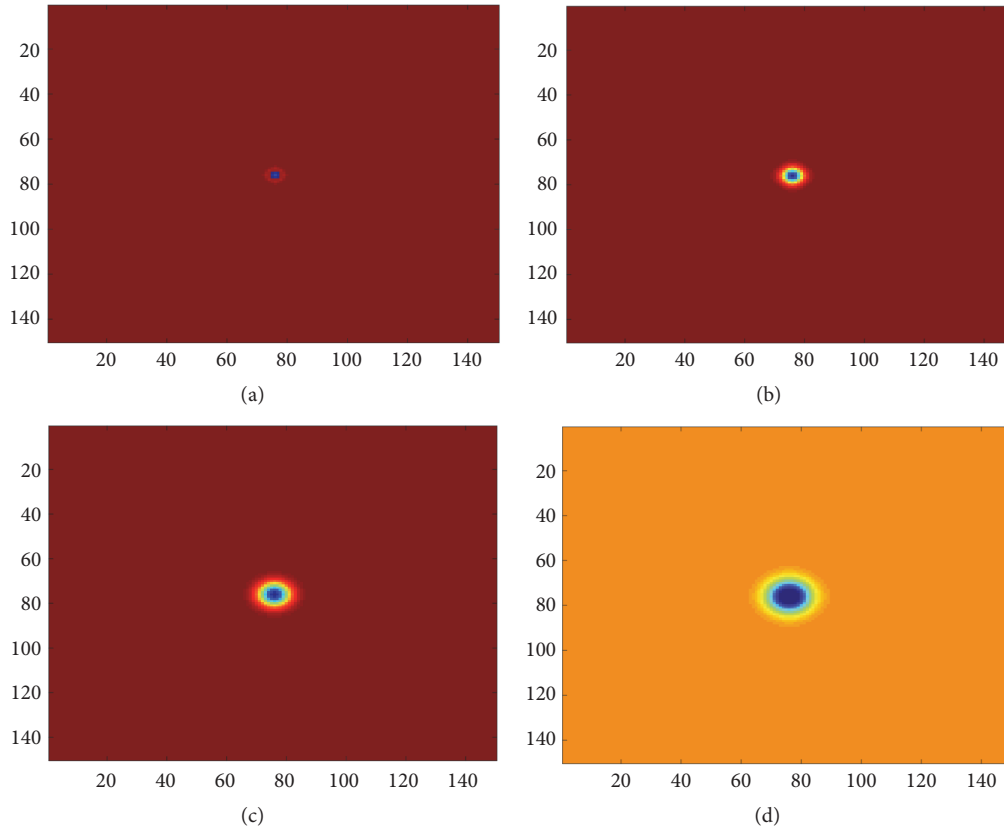
FIGURE 11: The snapshots of spatial distribution of membrane potential with color scale for neurons in the square array network for $k = 1$ and $D = 1$ at (a) $t = 2$ time units, (b) $t = 75$ time units, (c) $t = 170$ time units, and (d) $t = 300$ time units.

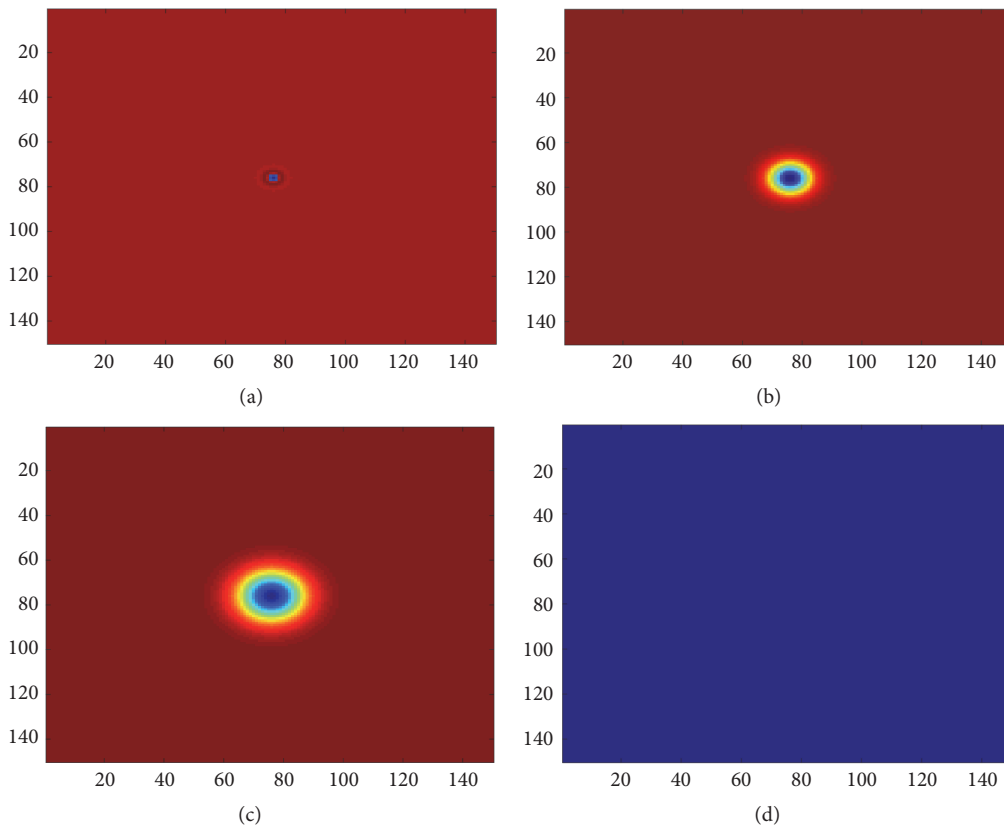

FIGURE 12: The snapshots of spatial distribution of membrane potential with color scale for neurons in the square array network for $k = 1$ and $D = 5$ at (a) $t = 2$ time units, (b) $t = 75$ time units, (c) $t = 135$ time units, and (d) $t = 300$ time units.

FIGURE 13: The snapshots of spatial distribution of membrane potential with color scale for neurons in the square array network for $k = 1.5$ and $D = 1$ at (a) $t = 2$ time units, (b) $t = 75$ time units, (c) $t = 170$ time units, and (d) $t = 300$ time units.
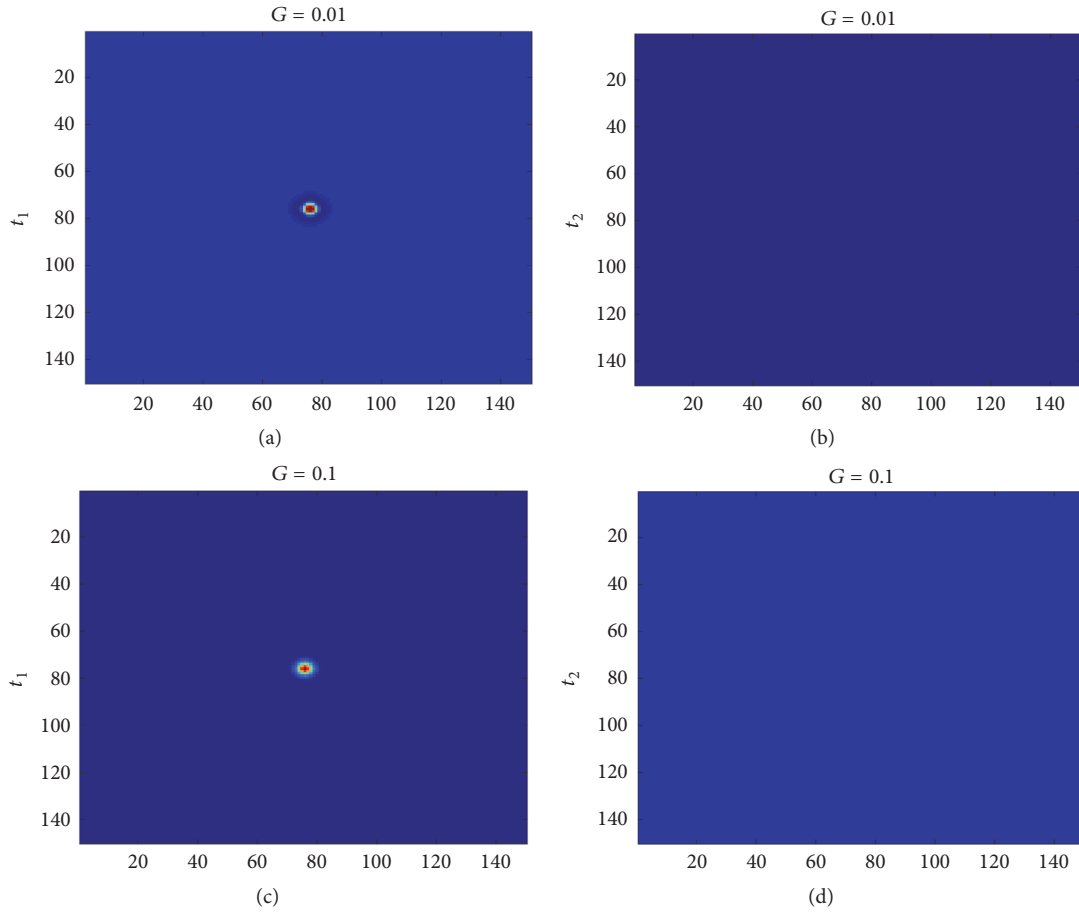

FIGURE 14: The snapshots of spatial distribution of membrane potential with color scale for neurons in the square array network for $k = 1.5$ and $D = 5$ at (a) $t = 2$ time units, (b) $t = 75$ time units, (c) $t = 135$ time units, and (d) $t = 300$ time units.

FIGURE 15: The snapshots of spatial distribution of membrane potential with color scale for neurons in the square array network for $k = 0$ and $D = 1$ at $t_1 = 2$ time units and $t_2 = 6$ time units. ((a), (b)) $G = 0.01$ and ((c), (d)) $G = 0.1$.

different collective behavior. Noticing the results before noise considerations, the coupling $k = 0.9$ was the only case with continuity of the central local area accompanied by sustained circular patterns. Our examination shows that, in opposition to the other memristor-type coupling levels, in this level the spatial representation is not robust against noise. Therefore, as is clear through the snapshots in Figure 19 the circular wave fronts change into some symmetrical deformations by increasing the noise intensity (see Figure 19(l)). In other words, the results reveal that the contribution of memristive effects denoting the synaptic plasticity determines the robustness of the excitable media against noise.

3.3. Numerical Results of Bifurcation Analysis.

Knowing that the dynamic behavior of a system can be revealed from its bifurcation analysis, in this subsection, the bifurcation analysis is carried out by setting different memristor-type couplings for a system of two coupled neuronal units. In this way, a qualitative analysis of the role of parameter k is available. We set $D = 1$. The numerical result can be found in Figure 22.

In Figure 22, it is shown that the system can switch over completely different dynamical behaviors under variation of memristor-type coupling. In accordance with the results represented in Sections 3.1 and 3.2, the whole diagram confirms that the system starts with periodic behavior, in which no propagation took place and then goes through some complicated behaviors, in which the two-dimensional lattice demonstrated wave propagation within multiple tiny rotating spiral seeds, and finally again it arrives at periodic dynamics, in which no propagation occurred.

In this paper, it was reported in Section 3.1 that the coupling intensity of $k = 0$, $k = 0.5$, $k = 1$, and $k = 1.5$ prevents the tissue from supporting wave propagation. Corresponding to these results, Figure 22 shows that the system undergoes periodic behavior by these mentioned memristor coupling intensities. Further, the chaotic behavior for $k = 0.7$ and $k = 0.8$ in Figure 22 concurs with the results in Figures 5 and 7, respectively, in which a turbulent electrical demonstration arose out of the respective memristor-type coupling intensities. Besides, in the previous subsections, the coupling intensity $k = 0.9$ was reported to be the only case significantly affected by the noise perturbation. In accordance with that, here our bifurcation analysis explains instability of the system in $k = 0.9$. Actually, the stability of the spatiotemporal pattern against noise is reduced when the neurons are set very close to their bifurcation point, which
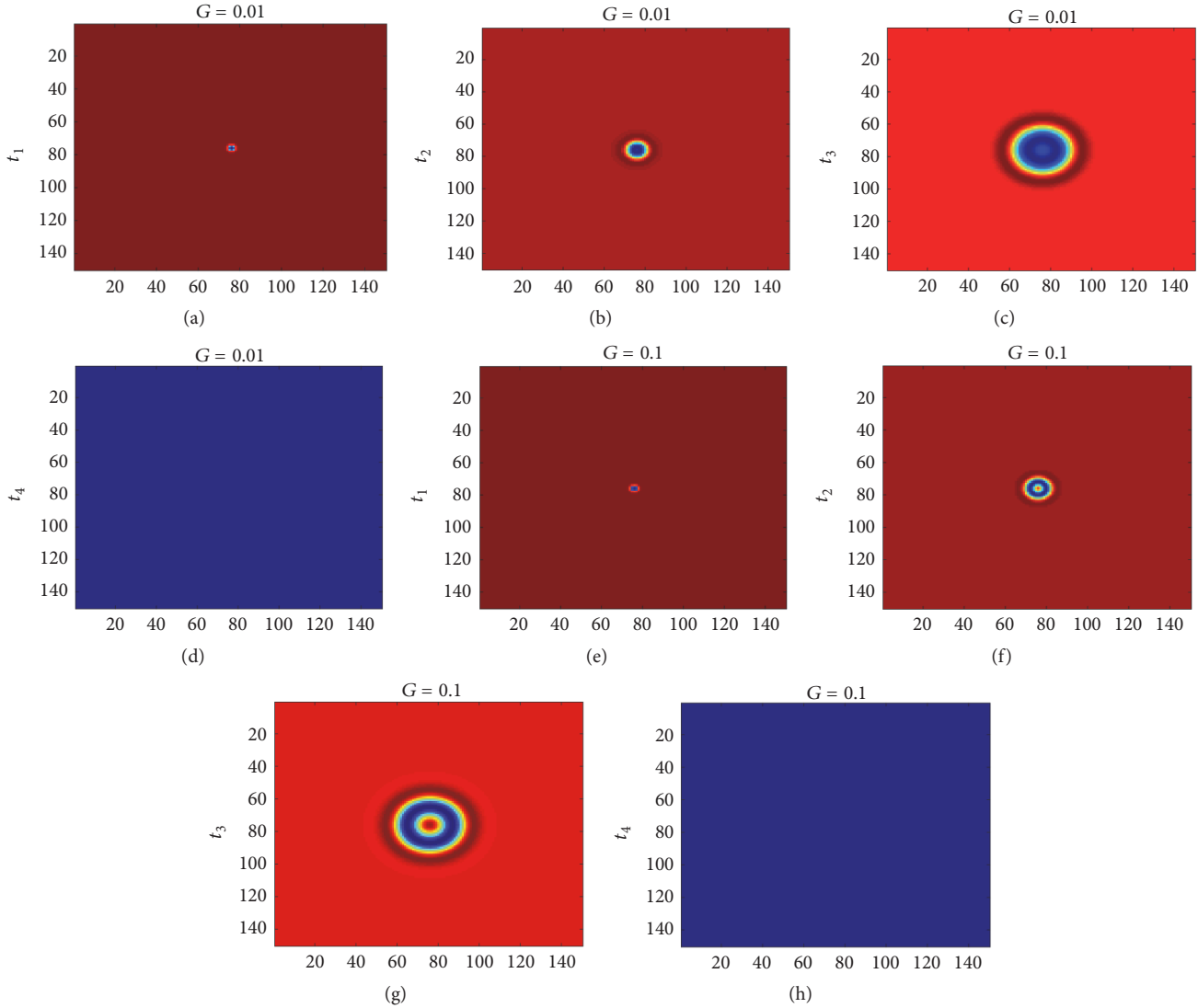
FIGURE 16: The snapshots of spatial distribution of membrane potential with color scale for neurons in the square array network for $k = 0.5$ and $D = 1$ at $t_1 = 2$ time units, $t_2 = 75$ time units, $t_3 = 170$ time units, and $t_4 = 300$ time units. ((a)–(d)) $G = 0.01$ and ((e)–(h)) $G = 0.1$.

is $k = 0.9$ (see Figure 23). At this point, the excitable media is very sensitive to perturbation. Thus, the media undergoes completely different dynamics in $k = 0.9$ by the noise impact.

4. Conclusion

In this study, the synaptic plasticity by means of memristor was investigated and the potential spatiotemporal patterns were detected. We showed that the memristive neuronal network is capable of representing plasticity phenomenon observed in biological cortical synapses. Excitable media were modeled by a network of 150×150 neuronal units with nearest neighbor connections containing memristor-type coupling. The 3-neuron Hopfield neuronal model was defined for the local dynamics of each unit. The tissue model was postulated to be capable of representing different dynamic behaviors mostly determined by the memristive properties. Our study showed that the level of memristive

effect plays a determinative role for the tissue to support wave propagation and also switch over different complex spatial demonstrations. In fact, the changes of dynamic law that govern the neurons within their connections were brought out from increasing or decreasing the memristor-type coupling strength. Although the resulting propagated waves could be expanded by greater amounts of resistor-type coupling, the total spatial pattern of the neurons did not change under the variation of resistor-type coupling. Further, we expanded our computations to investigate the stability of the resulting complex patterns against noise. It was revealed that all the spatial patterns were robust against noise impact except one case, in which the primary circular patterns changed into symmetrical deformations after the noise impact.

Finally, for further study, we sought to discover whether it is possible to find a meaningful relationship between the qualitative properties of the coupled neurons and the spatiotemporal demonstrations from a two-dimensional lattice.
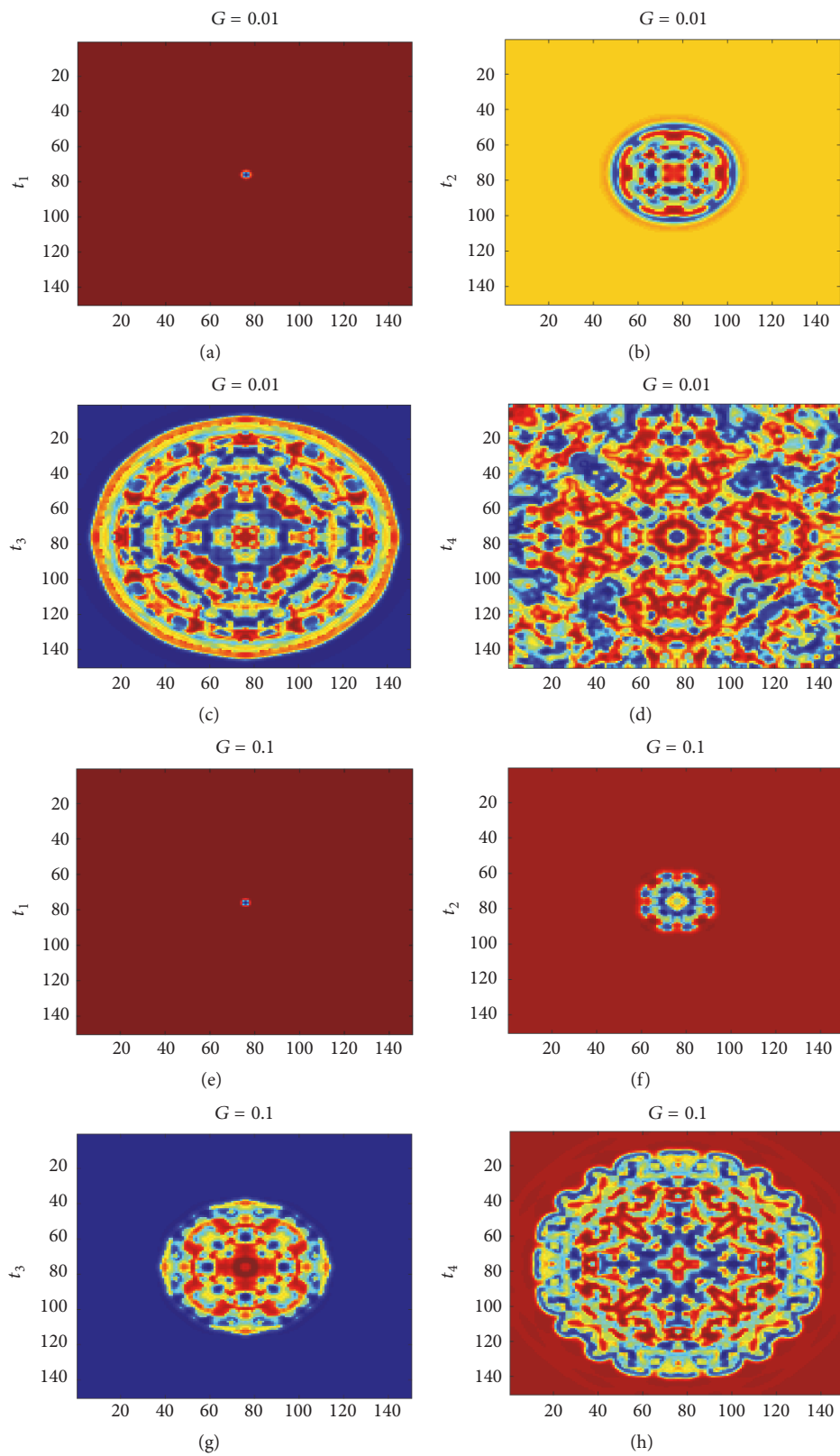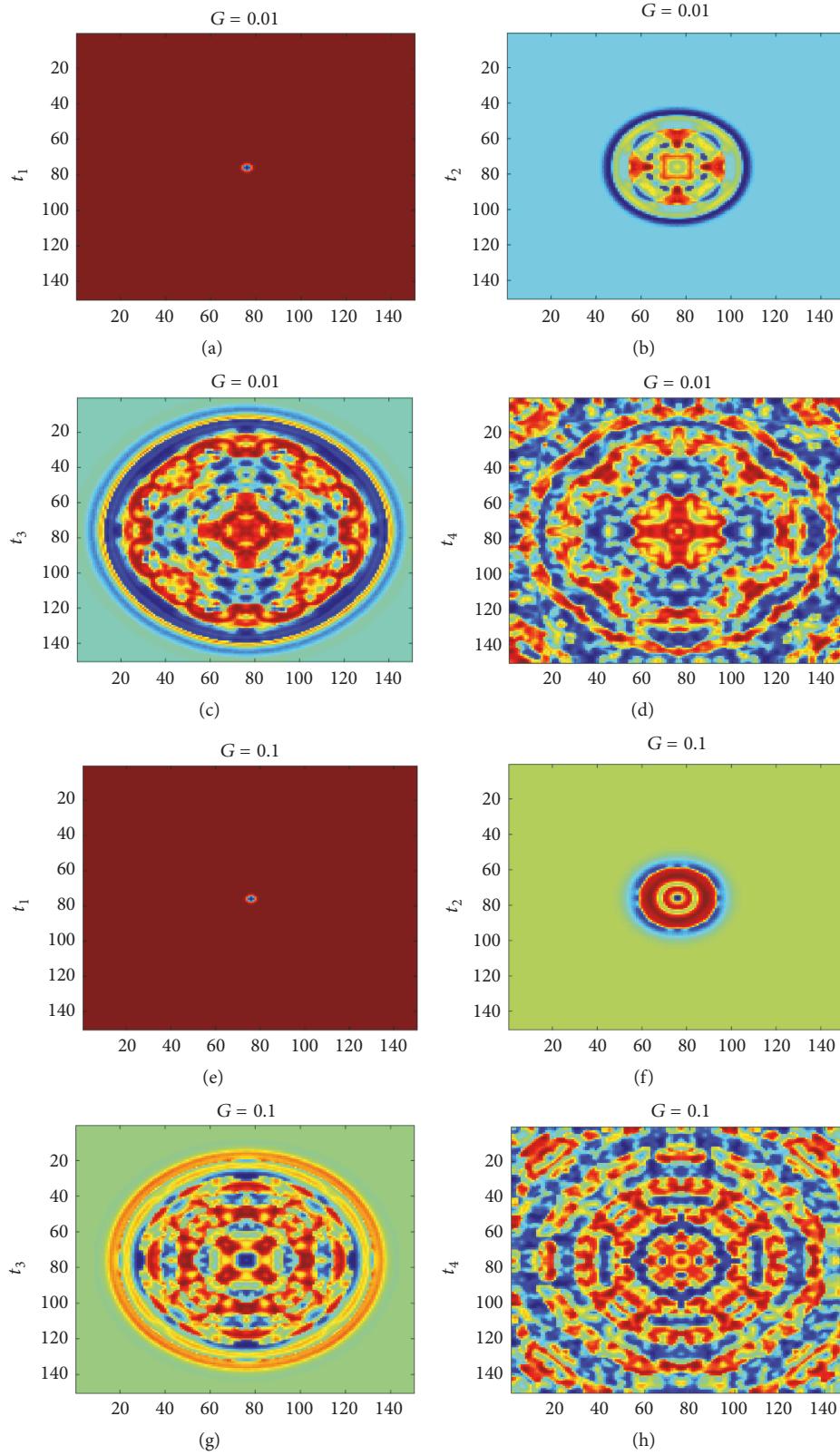
Figure 17: The snapshots of spatial distribution of membrane potential with color scale for neurons in the square array network for $k = 0.7$ and $D = 1$ at $t_1 = 2$ time units, $t_2 = 75$ time units, $t_3 = 170$ time units, and $t_4 = 300$ time units. ((a)–(d)) $G = 0.01$ and ((e)–(h)) $G = 0.1$.

FIGURE 18: The snapshots of spatial distribution of membrane potential with color scale for neurons in the square array network for $k = 0.8$ and $D = 1$ at $t_1 = 2$ time units, $t_2 = 75$ time units, $t_3 = 170$ time units, and $t_4 = 300$ time units. ((a)–(d)) $G = 0.01$ and ((e)–(h)) $G = 0.1$.
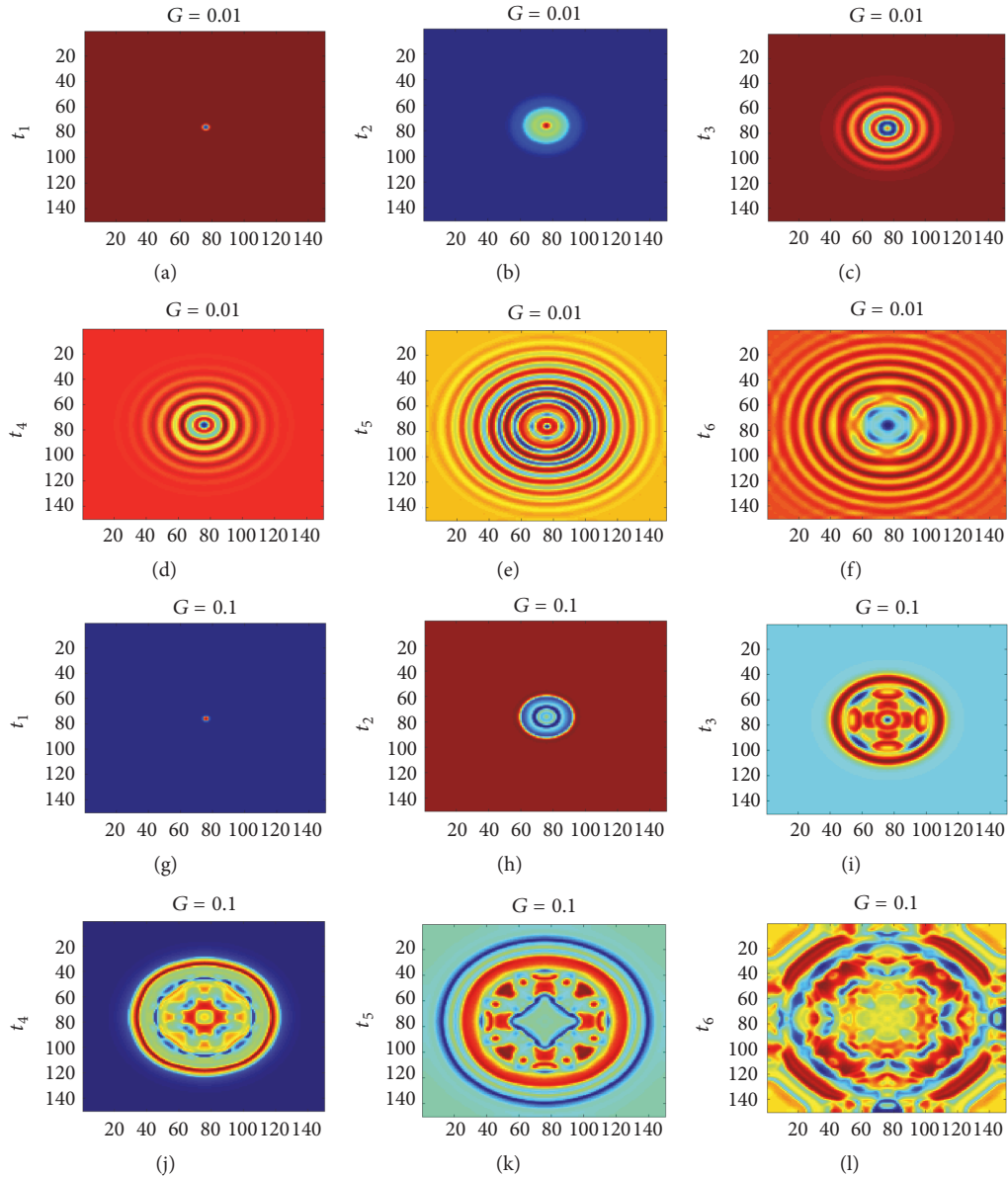
FIGURE 19: The snapshots of spatial distribution of membrane potential with color scale for neurons in the square array network for $k = 0.9$ and $D = 1$ at $t_1 = 2$ time units, $t_2 = 75$ time units, $t_3 = 170$ time units, $t_4 = 300$ time units, $t_5 = 450$ time units, and $t_6 = 600$ time units. ((a)–(f)) $G = 0.01$ and ((g)–(i)) $G = 0.1$.

Therefore, first the bifurcation analysis was carried out for different intensities of memristor-type coupling to see the possible mutual influence of the coupled neurons under memristive effects, and then the results were compared to our two-dimensional analysis. Our study revealed that the spatiotemporal patterns of electrical activity of the tissue concur with the bifurcation analysis. It was shown that the memristor coupling intensities, by which the system undergoes periodic behavior, prevent the tissue from holding wave propagation. In addition, the chaotic-like behavior in bifurcation diagram concurs with the turbulent spatiotemporal electrical activity of the tissue. Moreover, we showed that the excitable media is very sensitive to noise impact when the neurons are set close

to their bifurcation point, so that the spatiotemporal pattern is not stable.

Conflicts of Interest

The authors declare no conflicts of interest.
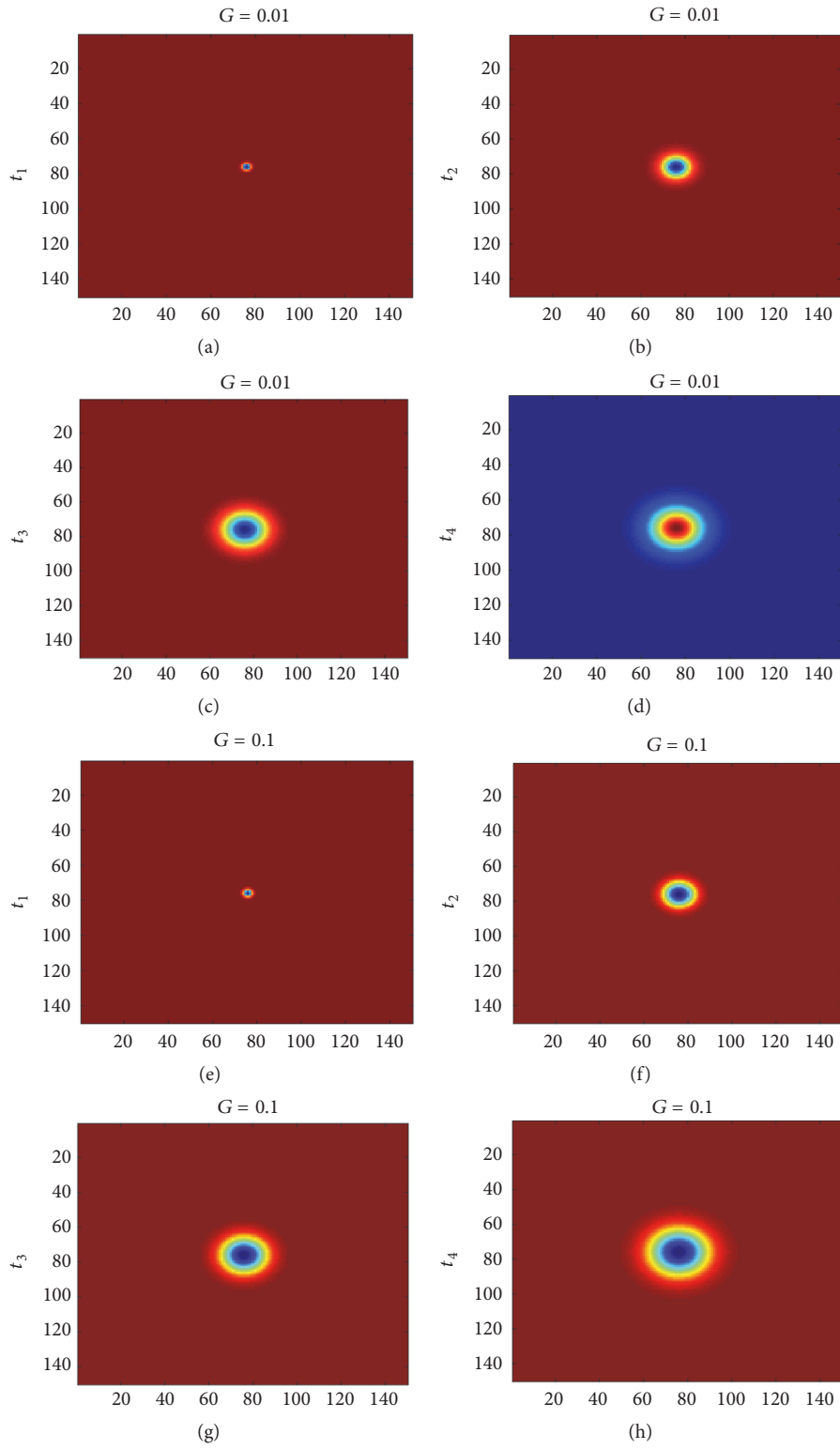
Acknowledgments

FIGURE 20: The snapshots of spatial distribution of membrane potential with color scale for neurons in the square array network for $k = 1$ and $D = 1$ at $t_1 = 2$ time units, $t_2 = 75$ time units, $t_3 = 170$ time units, and $t_4 = 300$ time units. ((a)–(d)) $G = 0.01$ and ((e)–(h)) $G = 0.1$.
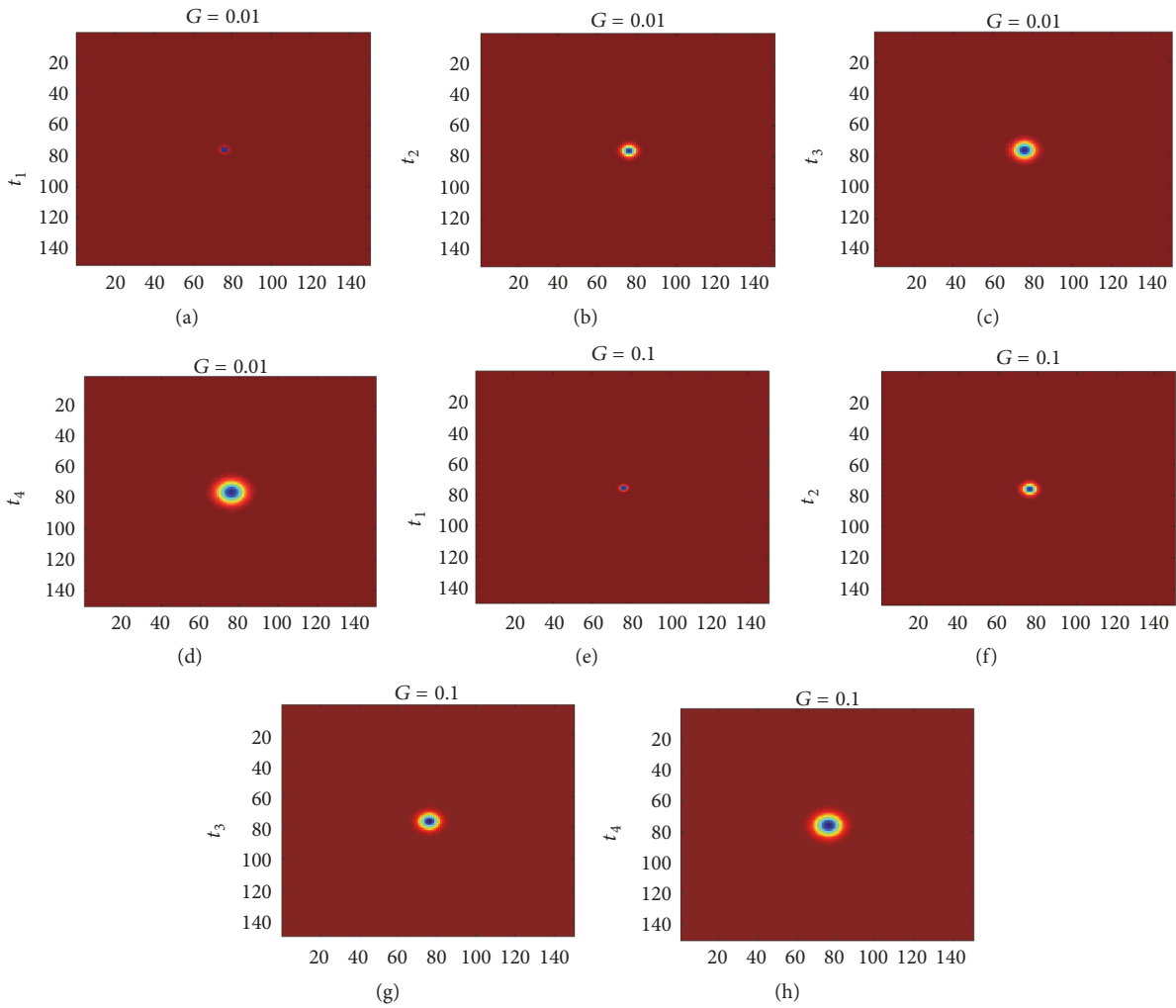
FIGURE 21: The snapshots of spatial distribution of membrane potential with color scale for neurons in the square array network for $k = 1.5$ and $D = 1$ at $t_1 = 2$ time units, $t_2 = 75$ time units, $t_3 = 170$ time units, and $t_4 = 300$ time units. ((a)–(d)) $G = 0.01$ and ((e)–(h)) $G = 0.1$.
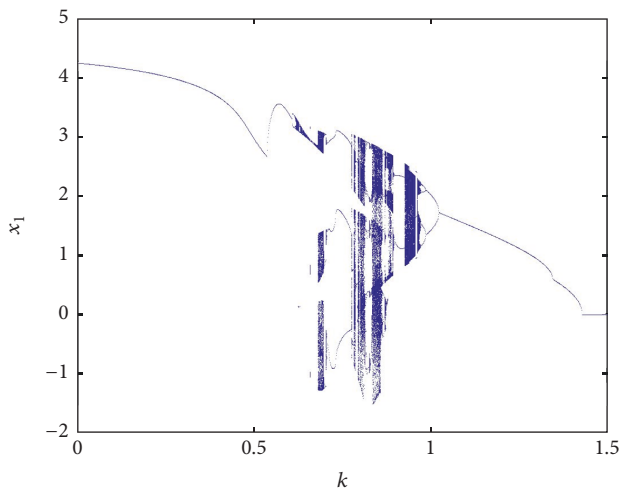

FIGURE 22: Bifurcation diagram of two coupled neurons for different memristor-type coupling intensities ($k = 0$ to $k = 1.5$), while $D = 1$ and other parameters are at their nominal values.
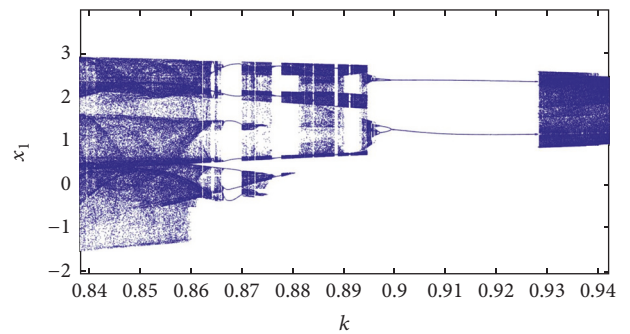

FIGURE 23: Bifurcation diagram of two coupled neurons for different memristor-type coupling intensities ($k = 0.84$ to $k = 0.94$), while $D = 1$ and other parameters are at their nominal values.

References

[1] J. Ma, F. Wu, and C. Wang, "Synchronization behaviors of coupled neurons under electromagnetic radiation," *International Journal of Modern Physics B*, vol. 31, no. 2, Article ID 1650251, 14 pages, 2017.

[2] S. Guo, J. Tang, J. Ma, and C. Wang, "Autaptic modulation of electrical activity in a network of neuron-coupled astrocyte," *Complexity*, vol. 2017, Article ID 4631602, 13 pages, 2017.

[3] E. R. Kandel, *Principles of Neural Science*, vol. 4, McGraw-hill, New York, NY, USA, 2000.

[4] L. Yu and Y. Yu, "Energy-efficient neural information processing in individual neurons and neuronal networks," *Journal of Neuroscience Research*, vol. 95, no. 11, pp. 2253–2266, 2017.

[5] E. A. Boroujeni and H. R. Momeni, "Non-fragile nonlinear fractional order observer design for a class of nonlinear fractional order systems," *Signal Processing*, vol. 92, no. 10, pp. 2365–2370, 2012.

[6] T. Kapitaniak, "Generating strange nonchaotic trajectories," *Physical Review E: Statistical, Nonlinear, and Soft Matter Physics*, vol. 47, no. 2, pp. 1408–1410, 1993.

[7] L. Yu, M. De Mazancourt, A. Hess et al., "Functional connectivity and information flow of the respiratory neural network in chronic obstructive pulmonary disease," *Human Brain Mapping*, vol. 37, no. 8, pp. 2736–2754, 2016.

[8] C. Wang, M. Lv, A. Alsaedi, and J. Ma, "Synchronization stability and pattern selection in a memristive neuronal network," *Chaos: An Interdisciplinary Journal of Nonlinear Science*, vol. 27, no. 11, Article ID 113108, 2017.

[9] J. Ma, H. Qin, X. Song, and R. Chu, "Pattern selection in neuronal network driven by electric autapses with diversity in time delays," *International Journal of Modern Physics B*, vol. 29, no. 1, Article ID 1450239, 2015.

[10] L. Yu and L. Liu, "Optimal size of stochastic Hodgkin-Huxley neuronal systems for maximal energy efficiency in coding pulse signals," *Physical Review E: Statistical, Nonlinear, and Soft Matter Physics*, vol. 89, no. 3, Article ID 032725, 2014.

[11] Y. Babacan and F. Kaçar, "Memristor emulator with spike-timing-dependent-plasticity," *AEÜ - International Journal of Electronics and Communications*, vol. 73, pp. 16–22, 2017.

[12] H. Kim, M. P. Sah, C. Yang, T. Roska, and L. O. Chua, "Neural synaptic weighting with a pulse-based memristor circuit," *IEEE Transactions on Circuits and Systems I: Regular Papers*, vol. 59, no. 1, pp. 148–158, 2012.

[13] S. P. Adhikari, C. Yang, H. Kim, and L. O. Chua, "Memristor bridge synapse-based neural network and its learning," *IEEE Transactions on Neural Networks and Learning Systems*, vol. 23, no. 9, pp. 1426–1435, 2012.

[14] E. Tlelo-Cuautle, L. G. de la Fraga, V.-T. Pham, C. Volos, S. Jafari, and A. D. J. Quintas-Valles, "Dynamics, FPGA realization and application of a chaotic system with an infinite number of equilibrium points," *Nonlinear Dynamics*, vol. 89, no. 2, pp. 1129–1139, 2017.

[15] V. T. Pham, S. Jafari, S. Vaidyanathan, C. Volos, and X. Wang, "A novel memristive neural network with hidden attractors and its circuitry implementation," *Science China Technological Sciences*, vol. 59, no. 3, pp. 358–363, 2016.

[16] D. B. Strukov, G. S. Snider, D. R. Stewart, and R. S. Williams, "The missing memristor found," *Nature*, vol. 453, pp. 80–83, 2008.

[17] L. O. Chua, "Memristor—the missing circuit element," *IEEE Transactions on Circuit Theory*, vol. 18, no. 5, pp. 507–519, 1971.

[18] L. O. Chua and S. M. Kang, "Memristive devices and systems," *Proceedings of the IEEE*, vol. 64, no. 2, pp. 209–223, 1976.

[19] Y. Babacan and F. Kaçar, "Floating memristor emulator with subthreshold region," *Analog Integrated Circuits and Signal Processing*, vol. 90, no. 2, pp. 471–475, 2017.

[20] C. K. Volos, A. Akgul, V.-T. Pham, and M. S. Baptista, "Anti-monotonicity, crisis and multiple attractors in a simple memristive circuit," *Journal of Circuits, Systems and Computers*, vol. 27, no. 2, Article ID 1850026, 2018.

[21] H. Bao, N. Wang, B. Bao, M. Chen, P. Jin, and G. Wang, "Initial condition-dependent dynamics and transient period in memristor-based hypogenetic jerk system with four line equilibria," *Communications in Nonlinear Science and Numerical Simulation*, vol. 57, pp. 264–275, 2018.

[22] J. Ma, Y. Xu, C. Wang, and W. Jin, "Pattern selection and self-organization induced by random boundary initial values in a neuronal network," *Physica A: Statistical Mechanics and its Applications*, vol. 461, pp. 586–594, 2016.

[23] J. Ma, L. Mi, P. Zhou, Y. Xu, and T. Hayat, "Phase synchronization between two neurons induced by coupling of electromagnetic field," *Applied Mathematics and Computation*, vol. 307, pp. 321–328, 2017.

[24] G.-Y. Zhang, J. Ma, L.-C. Yu, and Y. Chen, "Synchronization of spiral waves in a two-layer coupled inhomogeneous excitable system," *Chinese Physics B*, vol. 17, no. 11, pp. 4107–4113, 2008.

[25] F. Wu, C. Wang, W. Jin, and J. Ma, "Dynamical responses in a new neuron model subjected to electromagnetic induction and phase noise," *Physica A: Statistical Mechanics and Its Applications*, vol. 469, pp. 81–88, 2017.

[26] Y. Babacan, F. Kaçar, and K. Gürkan, "A spiking and bursting neuron circuit based on memristor," *Neurocomputing*, vol. 203, pp. 86–91, 2016.

[27] J. G. Howland and Y. T. Wang, "Synaptic plasticity in learning and memory: stress effects in the hippocampus," *Progress in Brain Research*, vol. 169, pp. 145–158, 2008.

[28] K. D. Cantley, R. C. Ivans, A. Subramaniam, and E. M. Vogel, "Spatio-temporal pattern recognition in neural circuits with memory-transistor-driven memristive synapses," in *Proceedings of the 2017 International Joint Conference on Neural Networks, IJCNN 2017*, pp. 4633–4640, USA, May 2017.

[29] T. Rinaldi, C. Perrodin, and H. Markram, "Hyper-connectivity and hyper-plasticity in the medial prefrontal cortex in the valproic acid animal model of autism," *Frontiers in Neural Circuits*, vol. 2, Article ID 4, 2008.

[30] J. A. Varela, K. Sen, J. Gibson, J. Fost, L. F. Abbott, and S. B. Nelson, "A quantitative description of short-term plasticity at excitatory synapses in layer 2/3 of rat primary visual cortex," *The Journal of Neuroscience*, vol. 17, no. 20, pp. 7926–7940, 1997.

[31] J.-V. Le Bé and H. Markram, "Spontaneous and evoked synaptic rewiring in the neonatal neocortex," *Proceedings of the National Acadamy of Sciences of the United States of America*, vol. 103, no. 35, pp. 13214–13219, 2006.

[32] M. S. El Naschie and T. Kapitaniak, "Soliton chaos models for mechanical and biological elastic chains," *Physics Letters A*, vol. 147, no. 5-6, pp. 275–281, 1990.

[33] S. Brezetskyi, D. Dudkowski, and T. Kapitaniak, "Rare and hidden attractors in Van der Pol-Duffing oscillators," *The European Physical Journal Special Topics*, vol. 224, no. 8, pp. 1459–1467, 2015.

[34] J. J. Hopfield, "Neurons with graded response have collective computational properties like those of two-state neurons," *Proceedings of the National Acadamy of Sciences of the United States of America*, vol. 81, no. 10, pp. 3088–3092, 1984.

[35] B. Bao, H. Qian, Q. Xu, M. Chen, J. Wang, and Y. Yu, "Coexisting behaviors of asymmetric attractors in hyperbolic-type memristor based hopfield neural network," *Frontiers in Computational Neuroscience*, vol. 11, no. 81, pp. 1–14, 2017.

[36] B. Bao, H. Qian, J. Wang et al., "Numerical analyses and experimental validations of coexisting multiple attractors in Hopfield neural network," *Nonlinear Dynamics*, vol. 90, no. 4, pp. 2359–2369, 2017.

[37] Y. Wang and J. Ma, "Bursting behavior in degenerate optical parametric oscillator under noise," *Optik—International Journal for Light and Electron Optics*, vol. 139, pp. 231–238, 2017.